Clim. Past Discuss., 5, 1659–1696, 2009
www.clim-past-discuss.net/5/1659/2009/

Climate of the Past Discussions

Climate of the Past Discussions is the access reviewed discussion forum of *Climate of the Past*

Northern high-latitude climate change between the mid and late Holocene – Part 2: Model-data comparisons

Q. Zhang[1,2], **H. Sundqvist**[1,3], **A. Moberg**[1,3], **K. Holmgren**[1,3], **H. Körnich**[1,2], and **J. Nilsson**[1,2]

[1]Bert Bolin Centre for Climate Research, Stockholm University, 10691 Stockholm, Sweden
[2]Department of Meteorology, Stockholm University, 10691 Stockholm, Sweden
[3]Department of Physical Geography and Quaternary Geology, Stockholm University, 10691 Stockholm, Sweden

Received: 11 June 2009 – Accepted: 16 June 2009 – Published: 25 June 2009

Correspondence to: Q. Zhang (qiong@misu.su.se)

Published by Copernicus Publications on behalf of the European Geosciences Union.

Abstract

The solar orbital forcing induced changes in insolation at the mid-Holocene compared to the late Holocene, which causes an amplification of the seasonal cycle in the Northern Hemisphere in the earlier period. The climate response over northern high latitudes, to this change in forcing has been investigated in three types of PMIP (Paleoclimate Modelling Intercomparison Project) simulations with different complexity of the climate system. The model results have also been compared with available reconstructions from temperature proxy data. Both the reconstructions and the PMIP2 models show a warm response in annual mean temperature, as well as in summer and winter temperature. The model-model comparisons indicate the importance of including the different physical feedbacks (ocean, sea-ice, vegetation) in the climate model. An objective selection method is applied in the model-data comparison to evaluate the capability of the climate model in reproducing the spatial response pattern. The comparisons between the reconstructions and the best-fit selected simulations show that over the northern high latitudes, summer temperature change follows closely to the insolation and shows a common feature with strong warming over land and relatively weak warming over ocean. A pronounced warming centre is found over Barents Sea in winter in model simulations, which is also supported by the nearby northern Eurasian continental reconstructions. The warming over Barents Sea corresponds to a positive North Atlantic Oscillation (NAO). The strengthened sea level pressure gradient may have caused a northward shift of the Atlantic storm track. It results in enhanced westerlies towards the northern Eurasia, which may be responsible for the winter warming over northern Fennoscandia and northern Siberia.

1 Introduction

To develop scenarios for possible future climate change from simulations with climate models is a major scientific challenge. The models need to be validated to assure

that they are able to reproduce observed climate change. Simulations of past climates allow evaluating how models respond to changes in external forcing such as solar orbital forcing and green-house gas. To undertake such evaluations, the Paleoclimate Modelling Intercomparison Project (PMIP) was launched (Joussaume and Taylor, 1995; Harrison et al., 2002), with a focus on two periods, the Last Glacial Maximum (LGM), 21 000 years ago, and the mid-Holocene (MH), 6000 years ago.

The mid-Holocene climate is reasonably well documented by proxy data and the main forcing compared to the late pre-industrial period is the insolation change due to the Earth's slowly changing orbit around the sun (Hewitt and Mitchell, 1996; Kutzbach et al., 1996; Vettoretti et al., 1998; Joussaume et al., 1999). During the mid-Holocene, the seasonal cycle of insolation forcing in the Northern Hemisphere was larger than today, with on average 5% more solar radiation in summer, and 5% less in winter (Berger, 1978). As a result of this change of insolation, a warmer summer and a colder winter could be expected over the northern high latitudes at the mid-Holocene compared to the late pre-industrial period. However, both the proxy reconstructions and climate model simulations reveal that the surface temperature not only responded to the solar forcing but also involved complex processes within the climate system such as ocean and land-surface feedbacks (Cheddadi et al., 1997; Wohlfahrt et al., 2004). Climate-model predictions of the response to anthropogenic changes in atmospheric composition suggest that the northern high latitudes are particularly sensitive to the radiative forcing mainly because of two positive feedbacks; changes in the extent of sea-ice cover, and changes in the albedo of the land surface as a consequence of changes in snow cover and the extent of forest (IPCC, 2007). Climate model simulations have shown that ice albedo feedbacks associated with variations in snow and sea-ice coverage are a key factor in positive feedback mechanisms which amplify climate change in northern high latitudes (Wohlfahrt et al., 2004; Renssen et al., 2005; Braconnot et al., 2007b). The polar amplification investigation under the double CO_2 scenario in the Coupled Model Intercomparison Projects (CMIP2) shows that, the range of simulated polar warming in the Arctic is between 1.5 to 4.5 times the global mean warming

(Holland and Bitz, 2003).The observational evidences from the last century are consistent with climate model simulations containing greenhouse gas concentrations (IPCC, 2007). Observations also show amplified warming in the Arctic, but its magnitude varies depending on time period analysed. Jones and Moberg (2003) found about 2.2 times larger warming in the Arctic compared to the global when the periods 1861–2000 and 1977–2001 were considered but only a factor of 1.2 for the period 1901–2000.

A variety of proxy records provide temporal and spatial information concerning climate change during the current interglacial, Holocene (Cheddadi et al., 1997; Prentice and Jolly, 2000; Kim and Schneider, 2004). For selected periods such as the mid-Holocene, intensive efforts have been dedicated to the synthesis of paleoclimatic observations and modelling intercomparisons (Liao et al., 1994; Harrison et al., 1998; Masson et al., 1999; Prentice et al., 1998; Guiot et al., 1999; Joussaume et al., 1999; Bonfils et al., 2004; Gladstone et al., 2005; Masson-Delmotte et al., 2006; Brewer et al., 2007). Most of the data-model comparisons are focused on proxy data rich area such as Europe. Existing data-model comparisons did not include the more recently completed PMIP2 simulations that include coupled ocean-atmosphere models and/or coupled ocean-atmosphere-vegetation models, which are generally in better agreement with the proxy data than the earlier PMIP1 simulations which were conducted with sea surface temperatures fixed to modern conditions (Braconnot et al., 2007a). The past and future polar amplification of climate change have been recently reviewed in both CMIP and PMIP simulations (Masson-Delmotte et al., 2006). The PMIP1 atmosphere-only simulations show no consistent temperature response for the polar regions to the mid-Holocene forcing, whereas the PMIP2 coupled atmosphere-ocean climate models systematically simulate a significant mid-Holocene warming both for Greenland (but smaller than ice-core based estimates) and Antarctica (consistent with the range of ice-core based range). The aim of this paper is to present a similar comparison but with focus on the northern high latitudes (60° N–90° N) where the collected proxy-based reconstructions are more numerous and cover a larger area than in previous comparisons. In a companion study (Sundqvist et al., 2009) we compile and analyse

the published quantitative proxy-based data climate reconstructions covering both the mid-Holocene (−6000 year BP; 6 ka) and preindustrial (AD 1750; 0ka) periods, to obtain and overview knowledge of the climate response documented in the paleoclimate records, as well as to high-light the uncertainty of the values in the reconstructions. In present paper, we use the database of PMIP1 (http://pmip.lsce.ipsl.fr/) and PMIP2 (http://pmip2.lsce.ipsl.fr/pmip2/) to perform a model-model and a model-data comparison. An optimal selection method (Goosse et al., 2006) is applied to measure the discrepancy between model results and reconstructions. This model-data comparison method aims to evaluate the capability of the climate models to reproduce the spatial climate response pattern seen in the proxy data, to find one (or a few) model simulation which most closely resembles the reconstructions. A further goal is to explore some feedback mechanisms responsible for mid- to late Holocene climate changes.

The paper is structured as follows. In Sect. 2, the temperature reconstructions for the northern hemisphere high latitudes from our companion paper (Sundqvist et al., 2009) are summarized. The PMIP simulations used in the current study are described in Sect. 3, while their temperature change during the mid-Holocene are presented in Sect. 4. The model data and the reconstructions are compared using a cost function in Sect. 5. Finally, conclusions are drawn in Sect. 6.

2 Evidence of the mid- to late Holocene climate change in reconstructions

The collection of proxy data used here, for comparison with climate model output, is discussed in detail in the companion paper by Sundqvist et al. (2009). Here, we summarize some of the main features of the proxy data and point out some main findings in the companion paper. This set of proxy-based reconstructions is obtained through a systematic scan for published calibrated temperature and precipitation reconstructions from the region north of 60° N, with data for both the 6 ka and 0 ka periods. Altogether, the selected proxy records are more numerous and cover a larger fraction of the entire area over northern high latitudes than previous data-model comparisons (Wohlfahrt

et al., 2004; Renssen et al., 2005; Masson-Delmotte et al., 2006). The climate change in mid- to late Holocene, as recorded in the proxy data, is defined as the 100-year average for two periods, that is, 6 ka minus 0 ka. More specifically, for the proxy data, this means the difference between the 100-year periods centered on 6000 years B.P. and 1750 AD.

Figure 1 shows the spatial distribution of the temperature reconstructions used in this study. In total there are 69 reconstructions used, including 48 July and August temperature reconstructions, 6 January temperature and 15 annual mean temperature reconstructions. The majority of reconstructions are from terrestrial archives, with a dominance of pollen, diatoms, and chironomids temperature proxies. A few borehole, ice-core, tree ring and speleothems are also included. The number of marine proxies is considerably smaller, only 5 including marine diatoms, alkenones and foraminifera from the North Atlantic ocean. Most reconstructions are located over the land areas neighboring the North Atlantic sector, with the highest density over Fennoscandia. There are, some proxy sites in Greenland and a few from the Northern Eurasian and North American continents. When compiling the reconstructions, the uncertainty from the calibration into temperature estimates done by the respective original authors, the uncertainty in temperature due to dating uncertainty, and (when applicable) the uncertainty due to errors in visual reading of temperature from graphs were considered and quantified in terms of a "total uncertainty" expressed by the standard deviation of the error. Detailed information about this uncertainty estimation is in Sundqvist et al. (2009). For practical reasons, July and August reconstructions are used to represent northern summer (JJA) mean temperature and, January reconstructions are used to refer to northern winter (DJF) mean temperature.

According to an unweighted average of all available temperature proxies, the averaged temperature change in the reconstructions from the northern high latitudes, indicates that the climate at 6 ka was 0.96±0.42°C warmer in summer, 1.71±1.70°C warmer in winter and 2.02±0.72°C warmer in annual mean temperature, in comparison to 0ka (Sundqvist et al., 2009). The uncertainties of the overall temperature change

CPD
5, 1659–1696, 2009

largely depend on the uncertainty in individual reconstructions and the number of reconstructions. For the winter temperatures, the uncertainty is almost equal to the estimated change.

The sparsity of the data distribution and the large uncertainty in winter temperature make the estimated change (warmer at 6 ka than at 0 ka) in winter temperature less reliable than the estimated changes in summer and annual mean temperatures. It has previously been noted, though, that in Europe warmer winter temperatures at 6 ka compared to 0 ka have been found in a majority of PMIP1 models and in proxy-based values (Masson et al., 1999). Such warmer winter temperatures at 6 ka cannot be explained by the insolation change directly, because the winter insolation in the high latitudes was lower in the mid-Holocene than at the present.

Another feature pointed out in the companion paper, is the observed larger change in the annual mean temperature change compared to winter and summer temperature changes in the reconstructions. One reason for this behavior could be that the proxy data used to reconstruct the annual temperature are not from the same archives as those for summer and winter temperature, resulting in the different location and the numbers of the data. Another reason could be the lack of a seasonal resolution in proxy data; hence we cannot exclude the possibility that the response in seasons for which we have no explicit data may have contributions to the change in annual mean temperature than the change in winter and summer. Furthermore, one can also not exclude the possibility that the transfer functions used to estimate the temperatures from proxy data are not sufficiently robust to allow a quantitative comparison between estimates for different seasons. Usually the reconstructions are not well resolved seasonally; therefore, the problem needs to be investigated further with the aid of climate model simulations that have reasonable physical constraints and appropriately prescribed external forcings corresponding to the particular past periods. In the following section we will first analyse PMIP database to obtain an estimate of the simulated climate response to the change in forcings and then we compare this with the results of the reconstructions.

3 The PMIP mid-Holocene simulations

The PMIP simulations used in this study include nineteen atmosphere only models with fixed SST (SSTf) from PMIP1 database, thirteen coupled ocean-atmosphere (OA) models and six coupled ocean-atmosphere-vegetation (OAV) models from the PMIP2 database. The models are presented with their names as specified in PMIP1 and PMIP2 databases, their spatial resolution and references to papers that describe the models in Table 1. For most of the modeling groups, the version of the coupled GCMs used for PMIP2 is identical to the version used for future climate change predictions in CMIP3, but with a lower resolution. Each model has been used to perform a mid-Holocene simulation (6 ka) and a pre-industrial control simulation (0 ka), under the same external forcings as required by the PMIP protocol. The main difference in forcing for mid-Holocene, compared to 0 ka, is set up by the orbital parameter, which is represented by the eccentricity, obliquity and precession. The PMIPs protocol also considers a change in the CH_4 concentration, with a lower concentration at 6 ka. The other greenhouse gases and the topography are the same in 6 ka and 0 ka simulations (Braconnot et al., 2007a) for each model. For the different models, the topography could be different due to the different horizontal and vertical resolution.

The PMIP1 atmosphere model with the fixed SST were integrated for 10-year long period, whereas the PMIP2 OA and OAV models were run to produce 100-year long simulations. Hence, all results presented here are computed from 10-year averages for PMIP1 simulations and 100-year averages for PMIP2 simulations. To compare with the reconstructions, rather than using single months (e.g. July or January), we use seasonal averages to represent season. Four seasonal mean for northern hemisphere is computed as the mean of the individual month, that is, December-January-February (DJF) mean for winter, March-April-May (MAM) mean for spring, June-July-August (JJA) mean for summer, and September-October-November (SON) mean for autumn (The proxy records, however, provide no spring and autumn information). The annual mean is computed from twelve monthly means.

In the present study the temperature from the model outputs refers to the surface air temperature at 2m height. The climate response to the change in insolation from the mid- to late Holocene is defined as the mean climate change between two time periods throughout the paper, i.e. 6 ka minus 0 ka. The three different types of models can help to identify the different responses in the climate system; the PMIP1 atmosphere only model simulations mainly show the direct atmospheric response; the PMIP2-OA simulations introduce the feedback from both ocean and sea ice; and the PMIP2-OAV simulations further introduce feedback from vegetation.

Note that we regard the simulations for the 0 ka conditions to be control runs. The results seen for the 6 ka simulations are thus interpreted as showing the response to the change in forcing compared to the control runs. Hence, for example, when we speak about a "warming" response in this paper, we mean that the simulation for the 6 ka period is warmer than the simulation for the 0 ka period.

4 Temperature change in PMIP simulations

The 6 ka orbital configuration leads to an increase of the amplitude of the annual cycle of the incoming solar radiation at the top of the atmosphere in the northern hemisphere and a decrease in the southern hemisphere. The insolation averaged over northern high latitudes (north of 60° N) shows a slight increase of about 2.9 W/m^2 for the annual mean, and a large increase by 23.5 W/m^2 for the JJA mean with a maximum increase of about 32 W/m^2 in July (Fig. 2). The DJF mean insolation shows a slight decrease by about −2.3 W/m^2 over the region. In the model simulations the modern calendar has been used for both periods instead of using a celestial based calendar as suggested by Joussaume and Braconnot (1997). The consequence is that change that occurring in autumn will be slightly underestimated over the northern hemisphere (Braconnot et al., 2007a).

The surface air temperature response to the insolation change is illustrated in figure.3 for the three types of PMIP models. In summer, all the PMIP1 and PMIP2

simulations show a warming at high latitudes in response to the enhanced summer insolation (Fig. 3c). In the PMIP1 atmosphere-only simulations, the atmospheric response produces a summer warming betweeb 0.3 to 1.6°C; the average for nineteen simulations is 0.84°C (Table 2). In the PMIP2 OA and OAV simulations, the response is more consistent (the spread is between 0.8 and 1.6°C) between the models than for PMIP1, except the OAV simulation with MRI-CGCM2.3.4nfa which has an anomalous 3.0°C. This suggests that dynamic response of the ocean and sea-ice in the PMIP2-OA narrow the inter-model spread of the summer warming compared to the PMIP1 simulations, for which the modern SST and sea ice fraction are prescribed. The averaged summer temperature change for the thirteen PMIP2-OA simulations is 1.10°C, i.e. about 0.26°C warmer than the PMIP1 results (Table 2). This difference between PMIP2-OA and PMIP1 simulations is primarily due to the reduced sea-ice cover, which induces well known sea-ice-albedo positive feedback. This positive feedback appears to be robust across all the thirteen PMIP2-OA simulations, as indicated by the small spread between models (Fig. 3c, middle panel). The average for the five PMIP2-OAV simulations shows a 0.20°C warmer response than the response in the PMIP2-OA simulations (Table 2), reflecting the amplification due to the vegetation feedback.

In accordance with the decreased insolation at 6 ka in the other three seasons (Fig. 2), the direct atmospheric response shows cooling in spring, autumn and winter in most of the PMIP1-SSTf simulations, with averaged values of −0.51°C, −0.12°C and −0.33°C respectively. As a result, there is no obvious change in annual mean temperature in the PMIP1-SSTf simulations. The feedback from the sea-ice does not appear to have any importance in spring, for which the atmospheric response to the insolation is dominant. This is suggested by the observation that no distinct differences in spring temperature response are found between the three types of PMIP simulations (Fig. 3b). Most of the PMIP1 and the PMIP2-OA simulations show cooling and the PMIP-OAV simulations show a slight cooling or no change at all in spring.

The influence of ocean and vegetation feedbacks on the surface air temperature appears to be more robust in autumn and winter. The average autumn warming in the

PMIP2-OA simulations is 1.35°C, i.e. which is about 0.25°C larger than the summer on average, indicating a lagged temperature response of the ocean to the enhanced summer insolation (Fig. 3a). The additional feedback from the vegetation in the PMIP2-OAV simulations further increase the autumn warming to 2.0°C (Fig. 3d, the anomalous MRI-CGCM2.3.4nfa simulation is not included in the average).

In winter, ten of the thirteen PMIP2-OA simulations and all the six PMIP2-OAV simulations show warming (Fig. 3a), whereas most of the PMIP1 simulations show a cooling (on average −0.33°C), the winter warming caused by the ocean feedback is 0.88°C, and the vegetation feedback causes another 0.67°C warming. Compared to the 0ka control simulation, the average winter warming reaches an average of 1.22°C in the PMIP2-OAV simulations.

From the Table 2, it can be concluded that the combined effects of orbital forcing, ocean feedback and vegetation feedback produce 1.30°C warming in summer, 2.00°C warming in autumn and 1.22°C warming in winter. The important feedbacks from ocean and vegetation take effect from summer to winter, but their effect is most important in autumn and winter. Together, they eventually translate into an annual mean temperature response of about 1.10°C. Strictly one can not separate the relative contribution from ocean or from vegetation simply by calculating the difference between the PMIP2-OAV and PMIP2-OA, because, for a given model, the OA and OAV simulations do not share the same control simulation. However, from the view of the model complexity, the OAV models are closer to the real climate world. The averaged temperature change in the OAV simulations is closer to the reconstructions than the OA and the PMIP1-SSTf simulations. It is clear that when the different feedbacks in the climate system are included in the climate model, the climate response is in better agreement with the proxy-based reconstruction.

In the above overall comparisons, the response varies from model to model in autumn and winter, i.e. when the ocean and vegetation feedbacks take a notable effect (Fig. 3a and d). This can be explained by the different ocean, sea-ice and vegetation physics are applied in the various PMIP2 models.

The most consistent response, across the models, is seen for the summer temperatures in the PMIP2-OA simulations (Fig. 3c). All thirteen simulations show between 0.8 and 1.6°C warming, with an average of about 1.0°C. We selected the six simulation with summer temperature responses closest in magnitude to the average and show their large scale patterns in Fig. 4. The main common feature in these simulations is characterized by increased temperature over almost the entire northern high latitudes. Corresponding to the direct responde to the insolation in summer, the warming over the continents is more pronounced than over the ocean, this feature is shown as the main temperature change pattern in the thirteen simulation ensemble illustration (not shown). However, the warming centres differ from model to model. For example, CCSM and CSIRO-Mk3L-1.1 have their maximum warming over North America and north Eurasia, as well as Greenland, whereas in MRI-CGCM2.3.4fa the warming over the Greenland is small. In the GISSmodeE and MIROC3.2 simulations, there is a small cooling area in the north Pacific and north Atlantic, respectively. An ensemble map may provide important information that reflects the inter-model consistency, but could also miss some regional features when averaging across the different model simulations. To find a realistic regional feature of the climate response, it seems necessary to select one (or a few) simulations that closely resemble the pattern seen in the proxy-based reconstructions. To achieve this goal, we applied a variant of the model-data comparison technique that was developed by Goosse et al. (2006), in order to select among the PMIP simulations the ones that minimize a cost function.

5 Model-data comparisons

The principle of the method used by Goosse et al. (2006) is to select among a relatively large ensemble of simulations, from one climate model, the one that is the closest to the observed climate. We have slightly adapted this simple data assimilation technique to suit our purposes, where our goal is to find the simulation(s) that objectively show(s) a best fit with the available proxy data. The selection is performed by comparing each

simulation to the available reconstructions in a consistent manner. The method is similar to the identification of analogues in meteorology, and it is expected to result in a good fit between model simulations and reconstructions at a reasonable cost. A main difference between our use of the method, and the approach of Goosse et al. (2006), is the case that we applied the objective selection method to an ensemble of model simulation with different models instead of an ensemble of simulations with a single model.

5.1 Selection of an optimal simulation

To select the best-fit simulation from the PMIP database, we applied a cost function CF:

$$\mathrm{CF}_k = \sqrt{\frac{1}{n}\sum_{i=1}^{n} w_i (T_{\mathrm{rec},i} - T^k_{\mathrm{mod},i})^2}$$

where CF_k is the value of the cost function for each PMIP simulation k. In our study, CF_k is calculated for summer, winter and annual mean. The quantity n in the summation, is the number of reconstructions used in the model-data comparison. $T_{\mathrm{rec},i}$ is the temperature change for reconstructions i, at a particular location. $T^k_{\mathrm{mod},i}$ is the value of the corresponding temperature change in the the PMIP simulation k for the model grid box that contains the location of the proxy-record i. Here we use the weights

$$w_i = \frac{1}{2\sigma_i}$$

where $2\sigma_i$ is the total uncertainty for reconstruction i (Sundqvist et al., 2009). This ensures that the reconstructions with a larger uncertainties to contribute less to the cost function.

The absolute value of the CF is meaningless, while the relative magnitude represents the goodness of each simulation compared to the other simulations. A low value

of the CF means that the simulated climate response pattern is close to the temperature change seen in the reconstructions, and the corresponding model is regarded to reproduce the reconstructed climate change better than the other models with higher CF values.

From the comparison of the different PMIP simulations in Fig. 3, and the overall findings in the companion paper by Sundqvist et al. (2009), it is evident that the PMIP2 simulations are overall in better agreement with the reconstructions than the PMIP1 simulations. The main reason for this is the better agreement in winter, where both the proxy data and the PMIP2 simulations agree on a warming at 6 ka compared to 0 ka. To evaluate the overall fitness of three types of PMIP simulations, the CF values of the ensembles for nineteen PMIP1-SStf simulations, thirteen PMIP2-OA simulations and six PMIP2-OAV simulations are calculated (Table 3). For summer temperature there are more reconstructions available and 50 data points (data from the same site have been averaged) are used to compute the CF. Only six data points are used to compute the CF for winter temperature change, and fifteen data points for annual mean. In Table 3 we found that summer CF-values are smaller than those of winter and annual mean. PMIP-OA ensemble has the lowest CF-value in summer, while PMIP-OAV ensemble has the lowest CF-value in winter and annual mean. It again objectively confirms that PMIP2 simulations are better in agreement with reconstructions. Particularly for winter and annual mean, PMIP-OAV simulations show the best agreement with data. Next we will calculate the CF-value for individual PMIP2 simulations and select the lowest one.

The CF values for each PMIP2 simulation is shown in Fig. 5, separately for the summer, winter and annual mean temperature changes. The separate calculation of CF-values for the different seasons allows separate identification of the models that fit best. The OAV simulation by MRI-CGCM2.3.4nfa is excluded since its CF-value for summer temperature is three times higher than the summer CF-value average.

For all PMIP2 models, except two of them, the CF-values are higher for the annual mean temperature changes than those for summer and winter temperatures (Fig. 5). This leads to some support for the suspicion that the larger change seen in the re-

constructions compared to those for summer and winter might indicate inconsistencies in the reconstructed changes of annual mean temperatures (see Sundqvist et al. (2009)). When comparing CF-values for summer and winter, it is observed that the summer CF-values are smaller for eleven of the eighteen models. Consistent with the overall comparisons, most PMIP2 models are better in summer temperature simulation with lower value of CF than those in winter and annual mean simulations (Fig. 5). This suggests that the simulated response to enhanced insolation in summer is robust and comparable across the most simulations, although two models have notably high summer CF-values. The results for winter is more variable, and four of the models have notably large CF-values. For summer temperatures (red curve in Fig. 5), five of the eighteen model simulations (CSIRO_Mk3L_1.0, CSIRO_Mk3L_1.1, MIROC3.2, MRI_CGCM2.3.4fa-OA and UBRIS_HadCM3M2-OA) have low CF values around 0.9 and are very close to each other. We interpret this as an indication that these models consistently well simulate the climate response to summer insolation forcing. However, the winter CF values in these simulations are not as good as the summer ones (green curve in Fig. 5). For example, the CF for MIROC3.2 and UBRIS_HadCM3M2-OA are the two with the highest CF values in winter. ECBILTCLIOVECODE and FOAM have the lowest CF values. The FOAM-OA simulation also shows low CF value in winter.

According to the CF values, the goodness-of-fit for the selected simulations is different in summer, winter and annual mean. A possible way to select the best-fit simulations is thus to combine the results for all seasons. Such a composition for summer, winter and annual mean temperature response is showed in black curve in Fig. 5. In general, the composite CF values show less discrepancies between models compared to the within-season results. Both the FOAM-OA and FOAM-OAV have relatively low CF values. Therefore, according to the composite CF value, the simulated climate response pattern in FOAM gives the best fit with reconstructions. MRI_CGCM2.3.4fa (OA and OAV), CSIRO_Mk3L_1.0, CSIRO_Mk3L_1.1 and ECBILTCLIOVECODE (OA and OAV) also show relatively low CF values. For FOAM, its OAV version shows a lower CF value than its OA version, indicating that the vegetation feedbacks in FOAM-

OAV further improve the results. The other four PMIP2-OAV simulations do not show much differences in CF value from their respective PMIP2-OA version.

In conclusion, it is not easy to identify a single model simulation which shows a best-fit with the proxy data. In the next section, we rather select two OAV models (FOAM and MRI CGCM2.3.4fa) that show overall relatively low CF-values for both summer and winter as well as the summer-winter-annual composite.

5.2 Large-scale change in surface temperature and related feedbacks

Figure 6 illustrates the change in surface temperature in the two PMIP-OAV simulations and in the reconstructions. For the simulated change in summer temperature, the main feature in both simulations is the remarkable land-sea contrast; the warming over Eurasia continent, North America and northern Scandinavia is much higher than over the ocean. One reconstruction data point over the Iceland shows cooling, and another two nearby data points show slightly warming, in two PMIP2-OAV simulations this region shows a rather small warming. Over the continents, the magnitude of the summer warming in FOAM-OAV is much stronger than in MRI_CGCM2.3.4fa-OAV, but it is closer to the magnitude of the reconstructions, especially those over Siberia and Scandinavia. Only one reconstruction from the North America supports the warm centre seen in FOAM-OAV and MRI_CGCM2.3.4fa-OAV.

Despite low CF values, the simulated changes in winter in the two simulations differ rather much from each other. This is not unexpected, given that all winter temperature proxy sites are located over only a small region including northern Scandinavia and northwestern Eurasia. This geographical spread of proxy sites is too small to constrain the model temperature response over much of the rest of the Arctic region.

FOAM-OAV shows winter warming over most of the land areas, except south of Greenland, while MRI_CGCM2.3.4fa-OAV shows notable cooling over much of North America and, to a smaller degree, over the southern parts of the Eurasian Arctic region. A striking feature in simulated winter temperature response is a strong warm region centered over Barents Sea in both simulations. The geographical extent of the

strongest warming is larger in FOAM-OAV compared to the other model; including in FOAM-OAV also northernmost Fennoscandia and the northwestern Eurasian continent. There are no winter temperature reconstructions available for the ocean, but the warming centered over Barents Sea seen in the simulations is reflected by those warming seen over Siberia and northern Fennoscandia in the reconstructions. In fact, this is the reason why these two simulations have low CF values for winter temperatures in Fig. 5.

The simulated change in annual mean temperatures is characterized by warming along the eastern sector of the Arctic ocean and Eurasian continent, with the warm centre located over Barents Sea, indicating a major contribution of the winter response. FOAM-OAV also shows a warming north Eurasia. In contrast, MRI_CGCM2.3.4fa shows cooling in part of this region and in much of North America. Again, the reason for such marked differences between the simulations is the lack of proxy data to constrain the models for these regions.

It is evident that the few proxy-data reconstructions for winter and annual mean temperatures cause large uncertainty in the model-data comparisons. Therefore, caution must be taken when attempting to attribute causes (in reality) for the warming response seen in the models, with a centre over Barents Sea. However, if this is also the true climate response, the exploration for more proxy data is needed to test the reliability of the measured response and for the examination of the possible mechanisms behind the response. Figure 7 shows the change in DJF mean sea level pressure in FOAM-OAV (Fig. 7a) and in MRI_CGCM2.3.4fa-OAV (Fig. 7b). A decreased pressure over the polar region and increased pressure over southern Europe in both simulations, indicating a mean shift towards a positive North Atlantic Oscillation (NAO). In the eastern part, the strengthened Siberian high and the weakened Arctic low, may have enhanced sea-level pressure gradients between the continent and the Arctic Ocean. Both the pressure gradients over the north Atlantic region and north Eurasia, may have driven the storm track further north, resulting in the warmer conditions over northern Fennoscandia and northeastern Eurasia (Thompson and Wallace, 1998).

CPD
5, 1659–1696, 2009

To further explore possible reasons for the simulated temperature changes, in Fig. 8 we show the change in seasonal variation of the sea ice fraction, the surface albedo and the ocean surface heat flux averaged over the high latitudes in FOAM-OA. It can be seen that, following the enhancement of the insolation in summer, the sea ice over the northern high latitudes is reduced all year around and has a maximum decrease by about 15% in August and September (Fig. 8a). An effect of the reduction of the sea-ice is a decrease of the surface albedo by about 10% in September (Fig. 8b). The surface ocean receives more heat during May to August directly from the enhanced summer insolation (Fig. 8c). Due to the reduced sea ice and surface albedo, ocean heat storage during summer is amplified. In September, following the decreased insolation over the northern high latitudes (Fig. 2), ocean starts to release the heat to the atmosphere. Therefore, the direct response of the ocean to the insolation, as well as the positive feedbacks from sea-ice albedo, lead to result that more heat flux being released from the ocean to the atmosphere in autumn and winter (Fig. 8c). These changes seen in simulate changes of the sea-ice, surface albedo and ocean surface heat flux are all possible mechanisms that can be responsible for the significant warming during autumn and winter in the Arctic region, as an indirect consequence of increased summer insolation.

6 Conclusions

We have performed model-model and model-data comparisons to examine the climate response to the change in insolation between the mid- and late Holocene. The comparison between 6 ka and 0 ka PMIP simulations shows that, at 6 ka, the orbital forcing of PMIP models leads to an increase by 23.5 W/m^2 of the insolation over northern high-latitudes (north of 60° N) in summer, and a slight decrease by −2.3 W/m^2 in winter over the same region. PMIP1 simulations, with fixed SST, show that the atmospheric response to this orbital forcing produces on average a 0.84°C warming in summer and a cooling in the rest of the year. In PMIP2 ocean-atmosphere coupled simulations,

the sea-ice-albedo feedback enhances the summer warming to 1.10°C, and the thermal inertia of the ocean leads to a 1.35°C warming in autumn and a 0.55°C warming in winter, while the cooling in spring remains the same as in the PMIP1 simulations. The PMIP2 ocean-atmosphere-vegetation coupled simulations also show warming in summer, autumn and winter; the changes being beyond 1.0°C in winter and summer, and reaching 2.0°C in autumn. When comparing these results with the temperature change seen in reconstruction from temperature proxy data (for summer, winter and annual mean), the results from the PMIP-OAV simulations are closer to the reconstructions. This indicates that when more physical feedbacks (ocean, sea-ice, vegetation) are included in the models, the climate response is in better agreement with the proxy-based reconstructions.

Based on an objective cost function approach, we selected two PMIP2-OAV model that show the best overall agreement with the available proxy data. The two models show a spatial response pattern that is largely consistent with the reconstructions in summer. For winter and the annual mean field, however, the geographical distribution of the proxy sites is too small to well constrain the models across the entire study region, leading to rather large differences between the response pattern seen in the two selected models for winter and annual mean data. The simulated summer temperature change follows closely from the insolation change and shows strong warming over land and relative weak warming over ocean. A pronounced warming center is found over Barents sea in winter, which is also supported by the nearby reconstructions from the northern Fennoscandia and northwestern Eurasia. The simulated winter warming over Barents Sea is found to correspond to a positive shift of the NAO. The strengthened sea level pressure gradients, which may have driven the storm track further north, and resulting in enhanced westerlies towards northern Eurasia. This hypothesized mechanism may be responsible for, or contribute to, the simulated winter warming seen over northern Fennoscandia and northeastern Eurasia.

Furthermore, analysis of one of the two selected best-fit OA models shows that in summer and early autumn, a 15% decrease in sea ice fraction leads to 10% percent

CPD
5, 1659–1696, 2009

decrease in surface albedo, which together with the ocean feedback, leads to about 1.2°C of summer temperature. During summer, the reduced sea ice and lowered surface albedo, enhance the warming over ocean, increase heat flux transfer from atmosphere to ocean and result in more heat storage in upper ocean. During autumn and winter, more heat flux is released from ocean to atmosphere and cause a significant warming in autumn and winter despite the weaker insolation. This result indicates that in the high latitude, the feedbacks in the climate system might be more important than the direct effect of the change in external forcing.

Acknowledgements. This work was undertaken within the project "Holocene climate variability over Scandinavia", at the Bert Bolin Centre for Climate Research in Stockholm University. We acknowledge the international modelling groups for providing their data for analysis and, the Laboratoire des Sciences du Climat et de l'Environnement (LSCE) for collecting and archiving the model data. The PMIP2/MOTIF Data Archive is supported by CEA, CNRS, the EU project MOTIF (EVK2-CT-2002-00153) and the Programme National d'Etude de la Dynamique du Climat (PNEDC). The analyses were performed using version 09-30-2008 of the database. More information is available on http://pmip2.lsce.ipsl.fr.

References

Berger, A. L.: Long-Term Variations of Daily Insolation and Quaternary Climatic Changes, J. Atmos. Sci., 35, 2362–2367, 1978. 1661

Bonfils, C., de Noblet-Ducoudré, N., Guiot, J., and Bartlein, P.: Some mechanisms of mid-Holocene climate change in Europe, inferred from comparing PMIP models to data, Clim. Dynam., 23, 79–98, 2004. 1662

Braconnot, P., Otto-Bliesner, B., Harrison, S., Joussaume, S., Peterchmitt, J.-Y., Abe-Ouchi, A., Crucifix, M., Driesschaert, E., Fichefet, T., Hewitt, C. D., Kageyama, M., Kitoh, A., Laîné, A., Loutre, M.-F., Marti, O., Merkel, U., Ramstein, G., Valdes, P., Weber, S. L., Yu, Y., and Zhao, Y.: Results of PMIP2 coupled simulations of the Mid-Holocene and Last Glacial Maximum - Part 1: experiments and large-scale features, Clim. Past, 3, 261–277, 2007a, http://www.clim-past.net/3/261/2007/. 1662, 1666, 1667

Braconnot, P., Otto-Bliesner, B., Harrison, S., Joussaume, S., Peterchmitt, J.-Y., Abe-Ouchi, A., Crucifix, M., Driesschaert, E., Fichefet, T., Hewitt, C. D., Kageyama, M., Kitoh, A., Loutre, M.-F., Marti, O., Merkel, U., Ramstein, G., Valdes, P., Weber, L., Yu, Y., and Zhao, Y.: Results of PMIP2 coupled simulations of the Mid-Holocene and Last Glacial Maximum - Part 2: feedbacks with emphasis on the location of the ITCZ and mid- and high latitudes heat budget, Clim. Past, 3, 279–296, 2007b, http://www.clim-past.net/3/279/2007/. 1661

Brewer, S., Guiot, J., and Torre, F.: Mid-Holocene climate change in Europe: a data-model comparison, Clim. Past, 3, 499–512, 2007, http://www.clim-past.net/3/499/2007/. 1662

Cheddadi, R., Yu, G., Guiot, J., Harrison, S. P., and Prentice, I. C.: The climate of Europe 6000 years ago, Clim. Dynam., 13, 1–9, 1997. 1661, 1662

Deque, M., Dreveton, C., Braun, A., and Cariolle, D.: The ARPEGE/IFS atmosphere model: a contribution to the French community climate modelling, Clim. Dynam., 10, 249–266, 1994. 1685

Gladstone, R. M., Ross, I., Valdes, P. J., Abe-Ouchi, A., Braconnot, P., Brewer, S., Kageyama, M., Kitoh, A., Legrande, A., Marti, O., Ohgaito, R., Otto-Bliesner, B., Peltier, W. R., and Vettoretti, G.: Mid-Holocene NAO: A PMIP2 model intercomparison, Geophys. Res. Lett., 32, L16707, doi:10.1029/2005GL023596, 2005. 1662

Goosse, H., Renssen, H., Timmermann, A., Bradley, R., and Mann, M.: Using paleoclimate proxy-data to select optimal realisations in an ensemble of simulations of the climate of the past millennium, Clim. Dynam., 27, 165–184, 2006. 1663, 1670, 1671

Gordon, C., Cooper, C., Senior, C. A., Banks, H., Gregory, J. M., Johns, T. C., Mitchell, J. F. B., and Wood, R. A.: The simulation of SST, sea ice extents and ocean heat transports in a version of the Hadley Centre coupled model without flux adjustments, Clim. Dynam., 16, 147–168, 2000. 1686

Gordon, C. T. and Stern, W. F.: A Description of the GFDL Global Spectral Model, Mon. Weather Rev., 110, 625–644, 1982. 1685

Gordon, H. B. and O'Farrell, S. P.: Transient Climate Change in the CSIRO Coupled Model with Dynamic Sea Ice, Mon. Weather Rev., 125, 875–908, 1997. 1685

Guiot, J., Boreux, J. J., Braconnot, P., Torre, F., and participants, P.: Data-model comparison using fuzzy logic in paleoclimatology, Clim. Dynam., 15, 569–581, 1999. 1662

Hack, J. J., Boville, B. A., Kiehl, J. T., Rasch, P. J., and Williamson, D. L.: Climate statistics from

the National Center for Atmospheric Research community climate model CCM2, J. Geophys. Res., 99, 20785–20813, 1994. 1685
Hall, N. M. J. and Valdes, P. J.: A GCM Simulation of the Climate 6000 Years Ago, J. Clim., 10, 3–17, 1997. 1685
Hansen, J., Sato, M., Ruedy, R., Lacis, A., Asamoah, K., Beckford, K., Borenstein, S., Brown, E., Cairns, B., Carlson, B., Curran, B., de Castro, S., Druyan, L., Etwarrow, P., Ferede, T., Fox, M., Gaffen, D., Glascoe, J., Gordon, H., Hollandsworth, S., Jiang, X., Johnson, C., Lawrence, N., Lean, J., Lerner, J., Lo, K., Logan, J., Luckett, A., McCormick, M. P., McPeters, R., Miller, R., Minnis, P., Ramberran, I., Russell, G., Russell, P., Stone, P., Tegen, I., Thomas, S., Thomason, L., Thompson, A., Wilder, J., Willson, R., and Zawodny, J.: Forcings and chaos in interannual to decadal climate change, J. Geophys. Res., 102, 25679–25720, 1997. 1685
Harrison, S., Braconnot, P., Hewitt, C., and Stouffer, R. J.: Fourth International Workshop of the Palaeoclimate Modelling Intercomparison Project (PMIP): Launching PMIP2 Phase II, EOS, 83, 447–447, 2002. 1661
Harrison, S. P., Jolly, D., Laarif, F., Abe-Ouchi, A., Dong, B., Herterich, K., Hewitt, C., Joussaume, S., Kutzbach, J. E., Mitchell, J., de Noblet, N., and Valdes, P.: Intercomparison of Simulated Global Vegetation Distributions in Response to 6 kyr BP Orbital Forcing, J. Climate, 11, 2721–2742, 1998. 1662
Harzallah, A. and Sadourny, R.: Internal Versus SST-Forced Atmospheric Variability as Simulated by an Atmospheric General Circulation Model, J. Climate, 8, 474–495, 1995. 1685
Hewitt, C. and Mitchell, J.: GCM Simulations of the Climate of 6 kyr BP: Mean Changes and Interdecadal Variability, J. Climate, 9, 3505–3529, 1996. 1661, 1685
Holland, M. M. and Bitz, C. M.: Polar amplification of climate change in coupled models, Clim. Dynam., 21, 221–232, 2003. 1662
IPCC: Climate Change 2007 – The Physical Science Basis: Working Group I Contribution to the Fourth Assessment Report of the IPCC (Climate Change 2007), Cambridge University Press, 2007. 1661, 1662
Jacob, R., Schafer, C., Foster, I., Tobis, M., and Andersen, J.: Computational Design and Performance of the Fast Ocean Atmosphere Model: Version 1, in: The 2001 International Conference on Computational Science, 175–184, 2001. 1686
Jones, P. D. and Moberg, A.: Hemispheric and Large-Scale Surface Air Temperature Variations: An Extensive Revision and an Update to 2001, J. Climate, 16, 206–223, 2003. 1662

Joussaume, S. and Braconnot, P.: Sensitivity of paleoclimate simulation results to season definitions, J. Geophys. Res., 102, 1943–1956, 1997. 1667

Joussaume, S. and Taylor, K. E.: Status of the Paleoclimate Modeling Intercomparison Project, in: Proceedings of the first international AMIP scientific conference, WCRP-92, 425–430, Monterey, USA, 1995. 1661

Joussaume, S., Taylor, K. E., Braconnot, P., Mitchell, J. F. B., Kutzbach, J. E., Harrison, S. P., Prentice, I. C., Broccoli, A. J., Abe-Ouchi, A., Bartlein, P. J., Bonfils, C., Dong, B., Guiot, J., Herterich, K., Hewitt, C. D., Jolly, D., Kim, J. W., Kislov, A., Kitoh, A., Loutre, M. F., Masson, V., McAvaney, B., McFarlane, N., de Noblet, N., Peltier, W. R., Peterschmitt, J. Y., Pollard, D., Rind, D., Royer, J. F., Schlesinger, M. E., Syktus, J., Thompson, S., Valdes, P., Vettoretti, G., Webb, R. S., and Wyputta, U.: Monsoon Changes for 6000 Years Ago: Results of 18 Simulations from the Paleoclimate Modeling Intercomparison Project (PMIP), Geophys. Res. Lett., 26, 859–862, 1999. 1661, 1662

K-1-Model-Developers: K-1 Coupled GCM (Miroc Description), Tech. rep., CCSR/NIES/FRCGC, 2004. 1686

Kim, J.-H. and Schneider, R.: GHOST global database for alkenone-derived Holocene sea-surface temperature records. http://www.pangaea.de/Projects/GHOST/, Tech. rep., DEKLIM, 2004. 1662

Kislov, A.: Three-dimensional model of atmospheric circulation with complete description of physical processes and simplified dynamics, Tech. rep., MSU, 1991. 1685

Kitoh, A., Noda, A., Nikaidou, Y., Ose, T., and Tokioka, T.: AMIP simulations of the MRI GCM, Pap Meteorol Geophy, 45, 121–148, 1995. 1685

Kutzbach, J., Bonan, G., Foley, J., and Harrison, S. P.: Vegetation and soil feedbacks on the response of the African monsoon to orbital forcing in the early to middle Holocene, Nature, 384, 623–626, 1996. 1661

Liao, X., Street-Perrott, F., and Mitchell, J.: GCM experiments with different cloud parameterization: comparisons with palaeoclimatic reconstructions for 6000 years BP, Data and Modelling, 1, 99–123, 1994. 1662

Marsland, S. J., Haak, H., Jungclaus, J. H., Latif, M., and Roske, F.: The Max-Planck-Institute Global Ocean/Sea Ice Model with Orthogonal Curvilinear Coordinates, Tech. Rep. 5, The Max-Planck-Institute, 2003. 1685

Marti, O., Braconnot, P., Bellier, J., Benshila, R., Bony, S., Brockmann, P., Cadule, P., Caubel, A., Denvil, S., Dufresne, J. L., Fairhead, L., Filiberti, M. A., Foujols, M.-A., Fichefet, T.,

Friedlingstein, P., Goosse, H., Grandpeix, J. Y., Hourdin, F., Krinner, G., Levy, C., Madec, G., Musat, I., deNoblet, N., Polcher, J., and Talandier, C.: The New IPSL Climate System Model: IPSL-Cm4, Note du Pole de Modelisation, Tech. Rep. 26, IPSL, 2005. 1686

Masson, V., Cheddadi, R., Braconnot, P., Joussaume, S., Texier, D., et al.: Mid-Holocene climate in Europe: what can we infer from PMIP model-data comparisons?, Clim. Dynam., 15, 163–182, 1999. 1662, 1665

Masson-Delmotte, V., Kageyama, M., Braconnot, P., Charbit, S., Krinner, G., Ritz, C., Guilyardi, E., Jouzel, J., Abe-Ouchi, A., Crucifix, M., Gladstone, R., Hewitt, C., Kitoh, A., LeGrande, A., Marti, O., Merkel, U., Motoi, T., Ohgaito, R., Otto-Bliesner, B., Peltier, W., Ross, I., Valdes, P., Vettoretti, G., Weber, S., Wolk, F., and YU, Y.: Past and future polar amplification of climate change: climate model intercomparisons and ice-core constraints, Clim. Dynam., 26, 513–529, 2006. 1662, 1664

McAvaney, B. and Colman, R.: The BMRC model : AMIP cofiguration, Tech. rep., BMRC Res Rep, 1993. 1685

McFarlane, N., Boer, G., Blanchet, J.-P., and Lazare, M.: The Canadian Climate Centre Second-Generation General Circulation Model and Its Equilibrium Climate, J. Climate, 5, 1013–1044, 1992. 1685

Modellbetreuungsgruppe, D.: The ECHAM 3 atmospheric general circulation model, Tech. Rep. 6, Deutsches Klimarechnenzentrum, Hamburg, Germany, 1994. 1685

Numaguti, A., Takahashi, M., Nakajima, T., and Sumi, A.: Development of atmospheric general circulation model, Tech. rep., Center for Climate System Research, University of Tokyo, Tokyo, 1995. 1685

Otto-Bliesner, B. L., Brady, E. C., Clauzet, G., Tomas, R., Levis, S., and Kothavala, Z.: Last Glacial Maximum and Holocene Climate in CCSM3, J. Climate, 19, 2526–2544, 2006. 1685

Petoukhov, V., Ganopolski, A., Brovkin, V., Claussen, M., Eliseev, A., Kubatzki, C., and Rahmstorf, S.: CLIMBER-2: a climate system model of intermediate complexity. Part I: model description and performance for present climate, Clim. Dynam., 16, 1–17, 2000. 1685

Phipps, S. J.: The CSIRO Mk3L Climate system model, Tech. rep., Antarctic Climate and Ecosystems CRC, University of Tasmania, Institute of Antarctic & Southern Ocean Studies, 2006. 1685

Prentice, C., Harrison, S. P., Jolly, D., and Guiot, J.: The climate and biomes of Europe at 6000 yr BP: comparison of model simulations and pollen-based reconstructions, Quaternary Sci. Rev., 17, 659–668, 1998. 1662

Prentice, I. C. and Jolly, D.: Mid-Holocene and glacial-maximum vegetation geography of the northern continents and Africa, J. Biogeography, 27, 507–519, 2000. 1662

Renssen, H., Goosse, H., Fichefet, T., Brovkin, V., Driesschaert, E., and Wolk, F.: Simulating the Holocene climate evolution at northern high latitudes using a coupled atmosphere-sea ice-ocean-vegetation model, Climate Dynamics, 24, 23–43, 2005. 1661, 1664, 1685

Roeckner, E., Bauml, G., Bonaventura, L., Brokopf, R., Esch, M., Giorgetta, M., Hagemann, S., Kirchner, I., Kornblueh, L., Manzini, E., Rhodin, A., Schlese, U., Schulzweida, U., and Tompkins, A.: The Atmospheric General Circulation Model Echam5, Part I: Model Description, Tech. rep., internal report 349, 2003. 1685

Sadourny, R. and Laval, K.: January and July performances of the LMD general circulation model, in: New perspectives in climate modeling, edited by Berger A, N. C., 179–198, Elsevier Amsterdam, 1984. 1685

Schlesinger, M. E., Andronova, N. G., Entwhistle, B., Ghanem, A., Ramankutty, N., Wang, W., and Yang, F.: Modeling and Simulation of Climate and Climate Change, In Past and present variability of the solar-terrestrial system: Measurements, data analysis and theoretical models, in: Proceedings of the International School of Physics Enrico Fermi, Course CXXXIII, edited by Cini Castagnoli, G. and Provenzale, A., 389–429, OS Press, Amsterdam, Varrena, Italy, 1997. 1685

Schmidt, G. A., Ruedy, R., Hansen, J. E., Aleinov, I., Bell, N., Bauer, M., Bauer, S., Cairns, B., Canuto, V., Cheng, Y., Del Genio, A., Faluvegi, G., Friend, A. D., Hall, T. M., Hu, Y., Kelley, M., Kiang, N. Y., Koch, D., Lacis, A. A., Lerner, J., Lo, K. K., Miller, R. L., Nazarenko, L., Oinas, V., Perlwitz, J., Perlwitz, J., Rind, D., Romanou, A., Russell, G. L., Sato, M., Shindell, D. T., Stone, P. H., Sun, S., Tausnev, N., Thresher, D., and Yao, M.-S.: Present-Day Atmospheric Simulations Using GISS ModelE: Comparison to In Situ, Satellite, and Reanalysis Data, Journal of Climate, 19, 153–192, 2006. 1686

Sundqvist, H., Zhang, Q., Moberg, A., Holmgren, H., and Kornich, H.: Northern high latitudes climate response to mid-Holocene insolation – Part I: Proxy data evidence, Clim. Past Discuss., accpeted, 2009. 1662, 1663, 1664, 1671, 1672, 1673

Thompson, D. W. J. and Wallace, J. M.: The Arctic Oscillation Signature in the Wintertime Geopotential Height and Temperature Fields, Geophys. Res. Lett., 25, 1297–1300, 1998. 1675

Thompson, S. L. and Pollard, D.: Greenland and Antarctic Mass Balances for Present and Doubled Atmospheric CO2 from the GENESIS Version-2 Global Climate Model, J. Climate,

10, 871–900, 1997. 1685
Tokioka, T., Yamazaki, K., Yagai, I., and Kitoh, A.: A description of the Meteorological Research Institute atmospheric general circulation model (MRI GCM-I), Tech. Rep. 13, MRI Tech. Report, 1984. 1685
Vettoretti, G., Peltier, W. R., and McFarlane, N. A.: Simulations of Mid-Holocene Climate Using an Atmospheric General Circulation Model, J. Climate, 11, 2607–2627, 1998. 1661
Wohlfahrt, J., Harrison, S., and Braconnot, P.: Synergistic feedbacks between ocean and vegetation on mid- and high-latitude climates during the mid-Holocene, Clim. Dynam., 22, 223–238, 2004. 1661, 1663
Yu, Y. Q., Zhang, X. H., and Guo, Y. F.: Global Coupled Ocean-Atmosphere General Circulation Models in Lasg/Iap, Adv. Atmos. Sci., 21, 444–455, 2004. 1686
Yukimoto, S., Noda, A., Kitoh, A., Hosaka, M., Yoshimura, H., Uchiyama, T., Shibata, K., Arakawa, O., and Kusunoki, S.: Present-Day Climate and Climate Sensitivity in the Meteorological Research Institute Coupled Gcm Version 2.3 (Mri-Cgcm2.3), J. Meteorol. Soc. Jpn., 84, 333–363, 2006. 1686

Table 1. PMIP models used in this study. The model name is listed as specified in PMIP database. Type A refers to an atmosphere-only model with fixed SST, OA refers to a coupled ocean-atmosphere and OAV refers to a coupled ocean-atmosphere-vegetation model. OA+OAV means the model has both simulations. Resolution of the spectral model is given by the type of truncation, the highest total wavenumber, and the number of levels, while for the grid models it is given in longitude(degree)× latitude(degree)×vertical levels.

Model name in PMIP database	Type	Resolution of Atmos Long×lat×level	Resolution of Ocean Long×lat×level	Reference
bmrc	A	R21L9		McAvaney and Colman (1993)
ccc2.0	A	T32L10		McFarlane et al. (1992)
ccm3	A	T42L18		Hack et al. (1994)
ccsr1	A	T21L20		Numaguti et al. (1995)
climber2	A	7°×10°×1		Petoukhov et al. (2000)
cnrm-2	A	T31L19		Deque et al. (1994)
csiro	A	R21L9		Gordon and O'Farrell (1997)
echam3	A	T42L19		Modellbetreuungsgruppe (1994)
gen2	A	T42L18		Thompson and Pollard (1997)
gfdl	A	R30L20		Gordon and Stern (1982)
giss-iip	A	5°×5°×9		Hansen et al. (1997)
lmcelmd4	A	5°×7°×11		Sadourny and Laval (1984)
lmcelmd5	A	4°×6°×11		Harzallah and Sadourny (1995)
mri2	A	4°×5°×15		Kitoh et al. (1995)
msu	A	10°×15°×3		Kislov (1991)
ugamp	A	T42L19		Hall and Valdes (1997)
uiuc11	A	4°×5°×14		Schlesinger et al. (1997)
ukmo	A	2°×4°×19		Hewitt and Mitchell (1996)
yonu	A	4°×5°×7		Tokioka et al. (1984)
CCSM	OA	T42L26	1°×1°×40	Otto-Bliesner et al. (2006)
CSIRO-Mk3L-1.0	OA	R21L18	2.8°×1.6°×21	Phipps (2006)
CSIRO-Mk3L-1.1	OA	R21L18	2.8°×1.6°×21	Phipps (2006)
ECBILTCLIOVECODE	OA+OAV	T21L3	3°×3°×20	Renssen et al. (2005)
ECHAM5-MPIOM1	OA	T31L19	1.875°×0.84°×40	Roeckner et al. (2003)
ECHAM53-MPIOM127-LPJ	OA+OAV	T31L19	1.875°×0.84°×40	Marsland et al. (2003)

Table 1. Continued.

Model name in PMIP database	Type	Resolution of Atmos Long×lat×level	Resolution of Ocean Long×lat×level	Reference
FGOALS-1.0g	OA	2.8°×2.8°×26	1°×1°×33	Yu et al. (2004)
FOAM	OA+OAV	R15L18	2.8°×2.8°×24	Jacob et al. (2001)
GISSmodelE	OA	4°×5°×17	4°×5°×17	Schmidt et al. (2006)
UBRIS-HadCM3M2	OA+OAV	3.75°×2.5°×19	1.25°×1.25°×20	Gordon et al. (2000)
IPSL-CM4-V1-MR	OA	3.75°×2.5°×19	2°×0.5°×31	Marti et al. (2005)
MIROC3.2.2	OA	T42L20	1.4°×0.5°×43	K-1-Model-Developers (2004)
MRI-CGCM2.3.4fa	OA+OAV	T42L30	2.5°×2.5°×23	Yukimoto et al. (2006)
MRI-CGCM2.3.4nfa	OA+OAV	T42L30	2.5°×2.5°×23	Yukimoto et al. (2006)

Table 2. Summary of seasonal changes in temperature (°C) averaged for nineteen PMIP1-SSTf simulations, thirteen PMIP2-OA simulations and five PMIP2-OAV simulations (excluding the MRI-CGCM2.3.4nfa simulation).

Forcing and feedbacks	MAM	JJA	SON	DJF	Annual
Orbital forcing	−0.51	0.84	−0.12	−0.33	−0.03
Orbital forcing+Ocean feedback	−0.46	1.10	1.35	0.55	0.64
Orbital forcing+Ocean feedback+vegetation feedback	−0.15	1.30	2.00	1.22	1.10

Table 3. Values of the cost function for nineteen PMIP1-SSTf ensemble, thirteen PMIP2-OA ensemble and six PMIP2-OAV ensemble.

Ensemble	Summer	Winter	Annual
PMIP1-SSTf	0.23	1.41	0.57
PMIP2-OA	0.16	1.25	0.44
PMIP2-OAV	0.18	0.98	0.41

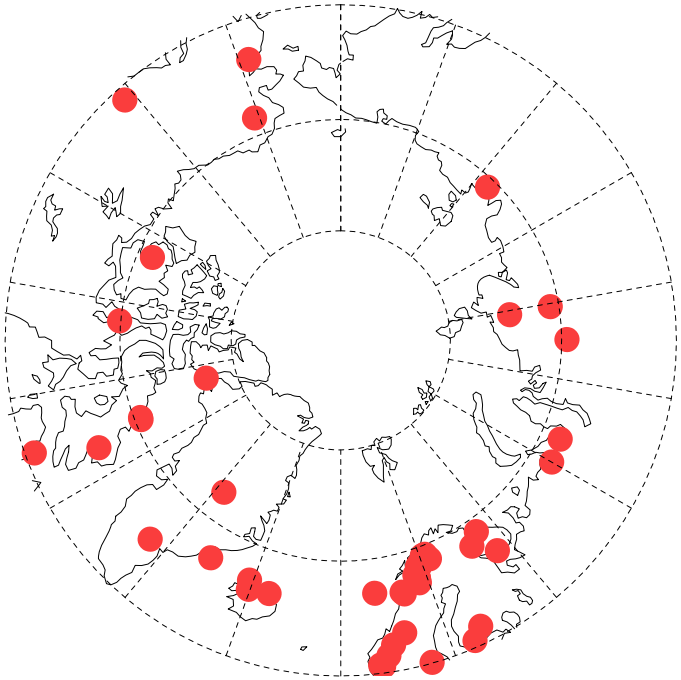

Fig. 1. Distribution of the temperature reconstructions from proxy data. In total, there are 69 reconstructions including 48 July and August temperature reconstructions, 6 January temperature and 15 annual mean temperature reconstructions.

CPD

5, 1659–1696, 2009

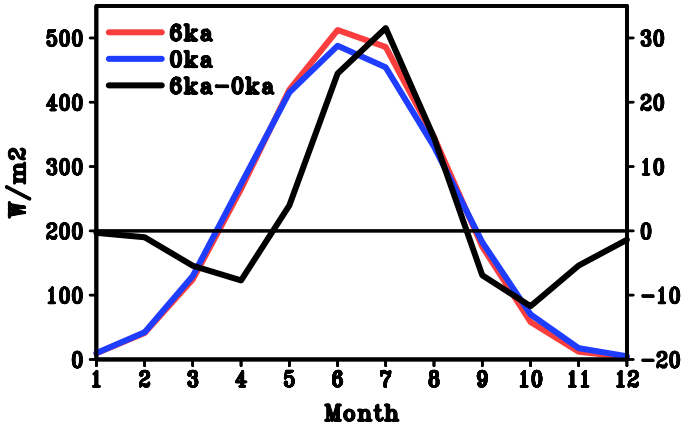

Fig. 2. The incoming solar radiation (W/m^2) at the top of the atmosphere averaged over 60° N–90° N for the mid-Holocene (6 ka, red), pre-industrial (0 ka, blue) and the difference between the two (6 ka–0 ka, black). The left-hand vertical axis refers to the absolute values and the right-hand scale to the difference values.

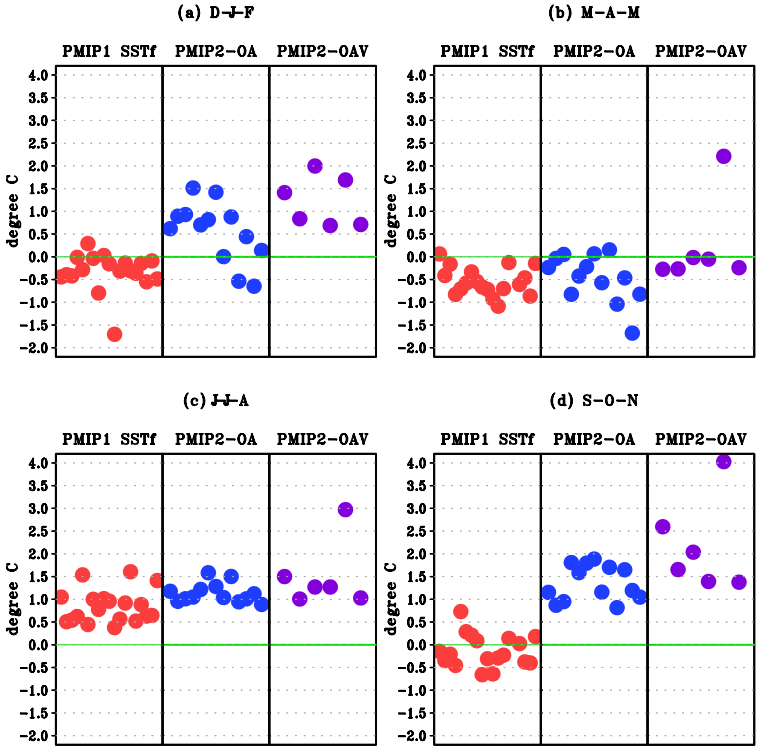

Fig. 3. Seasonal change in surface air temperature(°C) averaged over northern high latitudes (60° N–90° N) for the PMIP simulations. **(a)** DJF mean, **(b)** MAM mean, **(c)** JJA mean and **(d)** SON mean. The red circles are for PMIP1, the blue ones for PMIP2 OA and the purple ones for PMIP2 OAV.

CPD
5, 1659–1696, 2009

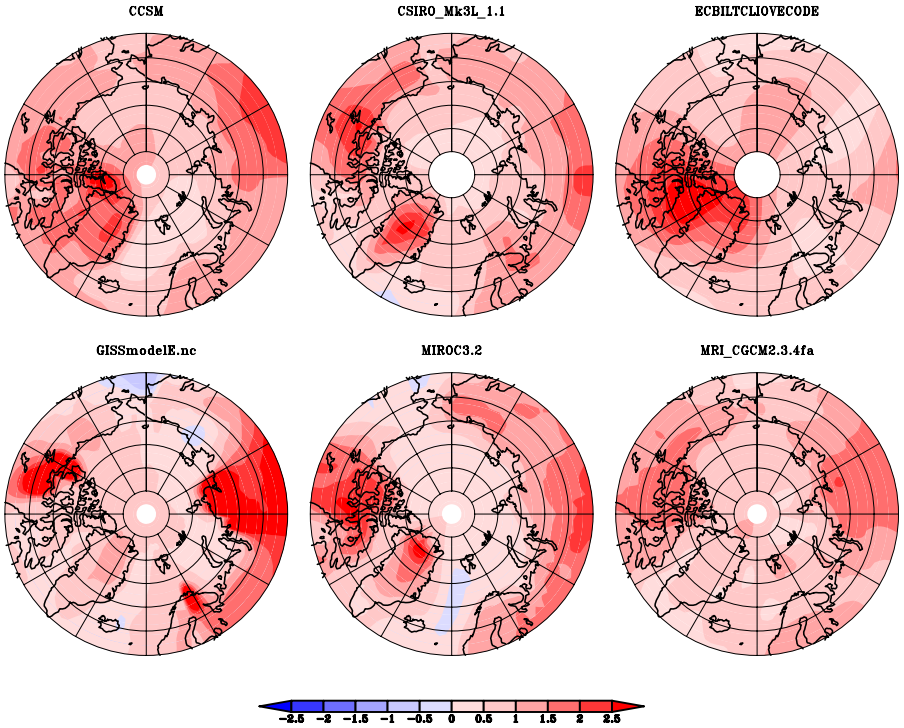

Fig. 4. Summer mean (JJA) change in surface temperature(°C) in six selected PMIP2-OA models.

CPD
5, 1659–1696, 2009

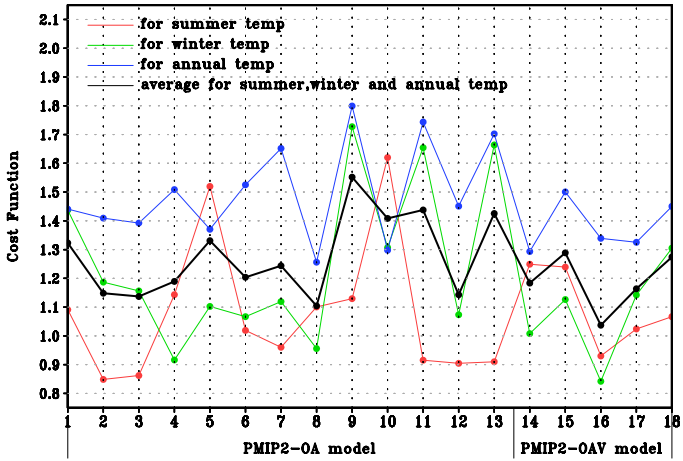

Fig. 5. Value of the cost function for the 18 PMIP2 models for summer temperature (red), winter temperature (green), annual mean temperature (blue), and a composition for summer, winter and annual temperatures (black). The values of the cost function is normalized by the number of the reconstructions. The horizonal X-axis indicates the 18 PMIP2 models used in the comparison. Number 1 to 13 are PMIP2-OA models: 1, CCSM; 2, CSIRO_Mk3L_1.0; 3, CSIRO_Mk3L_1.1; 4, ECBILTCLIOVECODE; 5, ECHAM5_MPIOM1; 6, ECHAM53_LPJ; 7, FGOALS_1.0g; 8, FOAM; 9, GISSmodelE; 10, IPSL_CM4_V1_MR; 11, MIROC3.2; 12, MRI_CGCM2.3.4fa; 13, UBRIS_HadCM3M2. Number 14 to 18 are PMIP2-OAV models: 14, ECBILTCLIOVECODE; 15, ECHAM53_LPJ; 16, FOAM; 17, MRI_CGCM2.3.4fa; 18, UBRIS_HadCM3M2.

CPD
5, 1659–1696, 2009

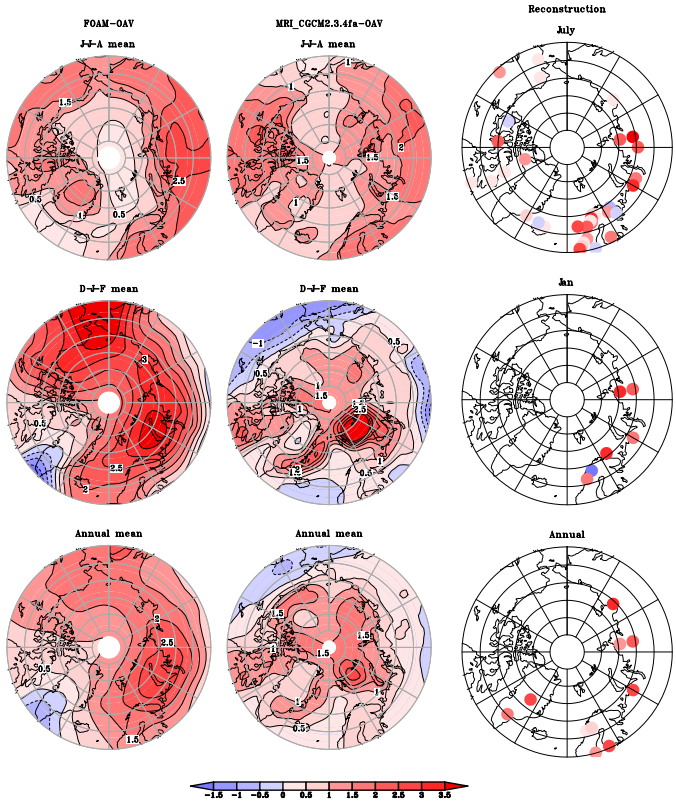

Fig. 6. The large scale pattern in surface temperature(˚C) change in FOAM-OAV (left column), MRI_CGCM2.3.4fa-OAV (middle column), and reconstructions (right column). Top row is for summer temperature, represented by JJA mean for model data and July temperature for reconstructions; middle row is for winter temperature, represented by DJF mean for model data and January temperature for reconstructions; bottom row is for annual mean temperature.

CPD
5, 1659–1696, 2009

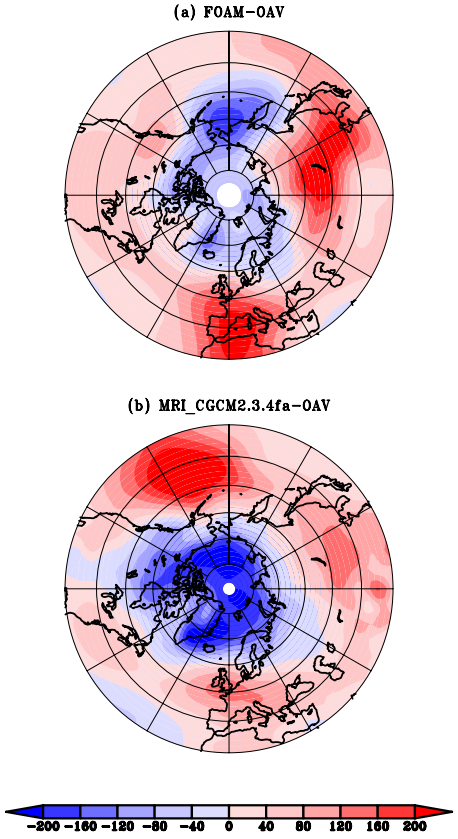

Fig. 7. The change in DJF mean sea level pressure (Pa) for **(a)** FOAM-OAV, **(b)** MRI_CGCM2.3.4fa-OAV.

CPD
5, 1659–1696, 2009

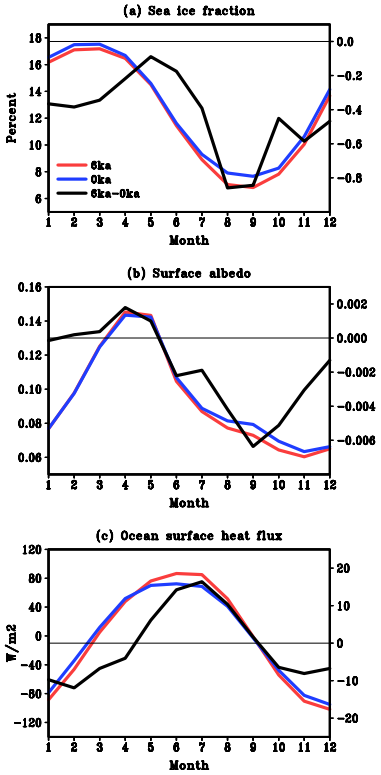

Fig. 8. Seasonal variation of **(a)** Sea ice fraction, **(b)** surface albedo and **(c)** ocean surface heat flux averaged over the 60° N–90° N latitudes in FOAM-OA. The left-hand vertical axis refers to the absolute values and the right-hand scale to the difference values.